

GALACTIC GLOBULAR CLUSTER RELATIVE AGES. II. ¹

Francesca De Angeli ¹, Giampaolo Piotto ¹, Santi Cassisi ², Giorgia Busso ³

Alejandra Recio-Blanco ⁴, Maurizio Salaris ⁵, Antonio Aparicio ⁶, Alfred Rosenberg ⁶

ABSTRACT

We present accurate relative ages for a sample of 55 Galactic globular clusters. The ages have been obtained by measuring the difference between the horizontal branch and the turnoff in two, internally photometrically homogeneous databases. The mutual consistency of the two data sets has been assessed by comparing the ages of 16 globular clusters in common between the two databases. We have also investigated the consistency of our relative age determination within the recent stellar model framework.

All clusters with $[\text{Fe}/\text{H}] < -1.7$ are found to be old, and coeval, with the possible exception of two objects, which are marginally younger. The age dispersion for the metal poor clusters is 0.6 Gyr (rms), consistent with a null age dispersion. Intermediate metallicity clusters ($-1.7 < [\text{Fe}/\text{H}] < -0.8$) are on average 1.5 Gyr younger than the metal poor ones, with an age dispersion of 1.0 Gyr (rms), and a total age range of ~ 3 Gyr. About 15% of the intermediate metallicity clusters are coeval with the oldest clusters. All the clusters with $[\text{Fe}/\text{H}] > -0.8$ are ~ 1 Gyr younger than the most metal poor ones, with a relatively small age dispersion, though the metal rich sample is still too small to allow firmer conclusions. There is no correlation of the cluster age with the Galactocentric distance. We briefly discuss the implication of these observational results for the formation history of the Galaxy.

Subject headings: Galaxy: evolution — Galaxy: formation — globular clusters: general

¹Dipartimento di Astronomia, Università di Padova, vicolo dell'Osservatorio 2, I-35122 Padova, Italy; deangeli, piotto@pd.astro.it

²INAF - Osservatorio Astronomico di Collurania, via Mentore Maggini, I-64100 Teramo, Italy; cassisi@te.astro.it

³Institut für Theoretische Physik und Astrophysik, Universität Kiel, Leibnizstrasse 15, D-24098 Kiel, Germany; busso@astrophysik.uni-kiel.de

⁴Dpt. Cassiopée, UMR 6202, Observatoire de la Côte d'Azur, BP 4229, 06304 Nice Cedex 4, France; arecio@obs-nice.fr

⁵Astrophysics Research Institute, Liverpool John Moores University, Twelve Quays House, Egerton Wharf, Birkenhead, CH41 1LD, UK; ms@staru1.livjm.ac.uk

⁶Instituto de Astrofísica de Canarias, Via Lactea, E-38200 La Laguna, Tenerife, Spain; antapaj, alf@iac.es

¹Based on observations with the NASA/ESA *Hubble Space Telescope*, obtained at the Space Telescope Science Institute, which is operated by AURA, Inc., under NASA contract NAS 5-26555, and on observations made at the European Southern Observatory, La Silla, Chile, and with the Isaac Newton Group Telescopes.

1. Introduction

Galactic globular clusters (GCs) play a key role in stellar astrophysics and cosmology. Stars in a given GC are to a good approximation coeval, were born with the same initial chemical composition, and are located approximately at the same distance from the observer. These characteristics make them valuable benchmarks for testing stellar evolution theories through comparisons of theoretical isochrones and luminosity functions with their observational counterparts (see, e.g. Renzini & Fusi Pecci 1988). In addition, due to the uniform age and initial chemical composition of stars belonging to a given cluster, the estimation of the cluster age is relatively straightforward, as shown in the pioneering work of Sandage & Schwarzschild (1952), Hoyle & Schwarzschild (1955).

Given that GCs are the oldest systems populating our Galaxy (and external galaxies) for which an age estimate is feasible, their ages provide a lower limit to the age of the Universe, whilst their relative ages (and possible correlations with metallicity, abundance patterns, and position) disclose fundamental information about Galactic formation mechanisms and timescales. Recent work on the age distribution of sizeable samples of GCs (Buonanno et al. 1998; Salaris & Weiss 1998; Rosenberg et al. 1999; VandenBerg 2000; Salaris & Weiss 2002) has led to a broadly consistent scenario in which metal poor clusters up to some intermediate metallicities are largely coeval, whereas at higher $[\text{Fe}/\text{H}]$ values an age spread exists, with possibly an age-metallicity relation. The age distribution with respect to the position within the Galaxy shows that an age spread is present at all distances, without any correlation with the distance from the Galactic centre (Rosenberg et al. 1999).

Unfortunately, absolute age measurements are still affected by a number of uncertainties, in particular by the large remaining errors on the GC distances and reddening (Gratton et al. 2003). Relative ages can be obtained with much higher accuracy by measuring the position of the main sequence turn-off (TO) – which is the most-used age indicator – relative to some other feature in the colour magnitude diagram (CMD) whose location is little or not at all dependent on age (Stetson, VandenBerg, & Bolte 1996, Sarajedini, Chaboyer, & Demarque 1997). However, any observed age indicator must be compared with theoretical predictions in order to derive an age. Uncertainties in both the input physics (Chaboyer et al. 1998), and the transformation from the theoretical to the observational plane (Buonanno et al. 1998), constitute a significant source of errors in the final age estimate, particularly when we want to compare ages of clusters with different metal content. In the present work, in order to minimise the uncertainties coming from the models, we used an updated set of theoretical tracks. More specifically, the theoretical isochrones employed in our analysis are the α -enhanced counterparts of the Pietrinferni et al. (2004) model and isochrone library, and have already been discussed briefly in Cassisi et al. (2004). The reliability and accuracy of this theoretical framework has already been tested by comparison with various empirical data sets by Riello et al. (2003) and by Salaris et al. (2004).

In the measurement of accurate relative ages, the photometric homogeneity of the data, and the homogeneity in the methods used to measure the age indicator parameters, are of fundamental importance, as we showed in Rosenberg et al. (1999), where, for the first time, we have been able to

measure relative ages on a truly photometrically homogeneous database for a large sample (34) of GCs. In this paper we intend to extend the work of Rosenberg et al. (1999), by adding a new, larger, photometrically homogeneous catalogue of CMDs, i.e. the HST snapshot catalogue by Piotto et al. (2002). For methodological consistency, we have also re-measured all the parameters relevant for an age estimate in the CMDs of Rosenberg et al. (2000a,b) used by Rosenberg et al. (1999).

The age-dating method used in our analysis is based on the magnitude difference ΔV_{TO-HB} (in the $F555W$ band for the HST data, and in the analogous V -Johnson band for the groundbased ones) between the TO and the horizontal branch (HB), i.e. the so called vertical method (Stetson et al. 1996; Sarajedini et al. 1997). The TO brightness is the age indicator (the TO gets fainter for increasing age) whereas the HB level is unaffected in the age range typical of GCs; this implies that older clusters display a larger value of ΔV_{TO-HB} . For ages around 10 Gyr the parameter ΔV_{TO-HB} scales approximately as $\delta\Delta V_{TO-HB}/\delta t \sim 0.1 \text{ mag Gyr}^{-1}$. Since it is a differential quantity, the comparison between observed and predicted ΔV_{TO-HB} values is unaffected by uncertainties in cluster reddening and distance modulus estimates, superadiabatic convection treatment in the stellar models as well as uncertainties in the colour-effective temperature relation adopted for transferring the models from the theoretical plane to the observational one. Another advantage of using the ΔV_{TO-HB} parameter as age indicator is that it is weakly sensitive to uncertainties in the cluster $[\text{Fe}/\text{H}]$, because at a fixed age the TO magnitude scales with $[\text{Fe}/\text{H}]$ almost like the HB level.

The plan of this paper is as follows. Section 2 describes the observational data, the measurement of the ΔV_{TO-HB} from the observed CMDs, and the estimate of the associated errors. Section 3 is devoted to the estimate of the age distribution of our cluster sample. A discussion of the main results is in Section 4. Conclusions are in Section 5.

2. Measurement of the observational parameters

2.1. The databases

The present investigation is based on two databases of GC CMDs:

- the HST snapshot database of Piotto et al. (2002);
- the groundbased database of Rosenberg et al. (2000a,b).

Each of the two databases is internally photometrically homogeneous. All the CMDs from both catalogues can be found at the Padova Globular Cluster Group web page (<http://dipastro.pd.astro.it/globulars>).

Here, for the first time, we present an age estimate based on the HST snapshot catalogue. This is a catalogue of CMDs for 74 Galactic GCs, observed in their central regions with the

WFPC2/HST camera in the photometric bands $F439W$ and $F555W$ (similar to the B , V in the Johnson-Cousins photometric system). For details about the observations, the reduction, and the photometric measurements please refer to Piotto et al. (2002).

The groundbased database has already been used for relative age measurements by Rosenberg et al. (1999), who selected the best CMDs from the two, photometrically homogeneous data sets collected, respectively, at the ESO/Dutch telescope (for the southern sky GCs) by Rosenberg et al. (2000b), and at the Isaac Newton Group Jacobus Kapteyn telescope (for the northern GCs) by Rosenberg et al. (2000a). For details about the observations, the reduction, and the photometric measurements please refer to Rosenberg et al. (2000a,b).

Forty one out of 74 clusters from the HST snapshot catalogue, and 30 out of 52 clusters from the groundbased catalogues, have a CMD which can be used for an age measurement. The remaining objects were excluded for several reasons: too shallow photometry, large field contamination, small number of member stars. Sixteen clusters are in common between the two catalogues, which allowed us to check the consistency of the ages derived from the two databases. Combining the two catalogues, we have been able to estimate ages for 55 GCs, representing more than 35% of the Galactic GC population. These GCs cover a metallicity interval $-2.3 < [\text{Fe}/\text{H}] < -0.3$, and are located from the very central part of the Galaxy out to ~ 30 kpc, therefore extending the metallicity and Galactocentric distance coverage of the original Rosenberg et al. (1999) paper.

In our attempt to be as homogeneous as possible, and consistent with our previous investigations based on the HST snapshot catalogue, we have adopted the metallicities listed in Rutledge et al. (1997) calibrated over both the Carretta & Gratton (1997, hereafter CG), as extended by Carretta et al. (2001), and Zinn & West (1984, hereafter ZW) metallicity scales. In this paper, we will present the results obtained adopting both metallicity scales. For those clusters that do not appear in the Rutledge et al. (1997) catalogue, we adopted the original ZW value when available. Otherwise, we calculated the ZW metallicity from Harris (1996, in the revised version of 2003) by fitting a straight line to the relation between the two scales. For clusters not in the Rutledge et al. (1997) compilation, $[\text{Fe}/\text{H}]$ values in the CG system were calculated from ZW values using the following equation (Carretta et al. 2001): $[\text{Fe}/\text{H}]_{CG} = 0.61 + 3.04[\text{Fe}/\text{H}]_{ZW} + 1.981[\text{Fe}/\text{H}]_{ZW}^2 + 0.532[\text{Fe}/\text{H}]_{ZW}^3$.

All the other cluster parameters used in this paper have been extracted from Harris (1996, in the revised version of 2003).

2.2. Measurement procedures

The relevant age indicator parameters described below have been extracted from both databases. It is worth emphasising the fact that the HST snapshot CMDs are in the $F439W$, $F555W$ WFPC2 flight system, while the groundbased CMDs are in the V , I Johnson-Cousins photometric system. Therefore, the vertical parameters obtained from the two databases cannot be directly compared. First, they must be compared with the theoretical models, transformed into the appropriate obser-

vational plane, for the age determinations. Only these final ages can be compared.

In order to apply the vertical method, we need to measure the magnitude of the TO point and the Zero Age Horizontal Branch (ZAHB) level.

For the TO measurement, we proceeded in the following way. First, the CMD of each clusters was cleaned by selecting stars based on the DAOPHOT PSF fitting parameters (CHI, SHA) and their photometric errors. Second, we extracted the fiducial main sequence (MS) for each cluster by taking the median of the colour distributions obtained in magnitude boxes containing a fixed number of stars, ranging from 40 to 250, depending on the total number of MS stars. A preliminary TO was then defined as the bluest point of the MS fiducial lines. For each cluster, we extracted a number of different MS fiducial lines by using different numbers of stars per box, and for each fiducial MS we associated a preliminary TO to its bluest point. Finally, we adopted as TO magnitude the mean value of all the preliminary TOs. The error on the mean of the preliminary TO magnitudes gave a first estimate of the error associated to the adopted TO magnitude. The TO magnitude error was then better quantified following the procedure explained in the next Section.

For the ZAHB magnitudes of the HST snapshot clusters, we adopted the values recently published by Recio-Blanco et al. (2005). They present distance moduli and reddening estimates for 72 Galactic globular clusters, based on the same photometric catalogue we are using here. The ZAHB magnitudes were estimated starting from the RR Lyrae level, for low and intermediate metallicity clusters, and from the fainter envelope of the red HB, for metal rich ones. For a detailed description of the adopted method, please refer to Recio-Blanco et al. (2005). Here it suffices to say briefly that:

- the ZAHB level for *metal rich clusters* ($[\text{Fe}/\text{H}] \geq -1.0$) was set as the magnitude of the lower envelope of the HB minus 3 times the photometric error (resulting from artificial star experiments) at that magnitude;
- for *low and intermediate metallicity clusters* ($[\text{Fe}/\text{H}] < -1.0$), a template cluster with similar metallicity and with a sizeable population of RR Lyrae stars was selected from the literature. Five different templates were used to cover the entire metallicity range. The CMD of the template cluster was shifted in colour and magnitude until its HB overlapped the HB of the cluster whose ZAHB level was to be determined. This procedure allowed to obtain the mean apparent magnitude of the cluster RR Lyrae stars which was then transformed into the apparent ZAHB magnitude by using the relation (Cassisi & Salaris 1997):

$$V_{\text{ZAHB}} = V_{\text{RR Lyrae}} + 0.152 + 0.041[\text{M}/\text{H}]. \quad (1)$$

For methodological consistency, we repeated the measures of the TO and ZAHB magnitudes also for the groundbased CMDs. The TO measurement method by Rosenberg et al. (1999) is very similar to what we did in the present paper, while the approach to obtaining the ZAHB magnitudes is completely different. The new ZAHB magnitudes for the groundbased CMDs have been measured

exactly as described above for the HST data, and in more detail by Recio-Blanco et al. (2005). For the groundbased low and intermediate metallicity clusters we used the same templates as for the HST ones. However, the reference CMDs are different, as the groundbased catalogue is in the V , I photometric system. Table 1 lists the reference clusters, the metallicity range of the comparison clusters, and the source of the photometry for the reference CMDs.

Figures 1 and 2 show two examples of our results. The CMDs of two clusters are shown, one from the groundbased catalogue (NGC 6218) and one from the the snapshot database (NGC 362). In Fig. 1, the brighter part of the CMD of one of the templates used for the ZAHB measurements is also shown. The template is NGC 5904. NGC 6218 has a quite scarcely populated HB, nevertheless by applying our technique we were able to estimate the ZAHB magnitude. We would like to emphasise the fact that NGC 6218 is also contained in the snapshot catalogue and ZAHB measurements were made on the HST CMD and published by Recio-Blanco et al. (2005). Those measurements are in excellent agreement with those obtained from the groundbased CMD, considering the different but similar bandpasses.

2.3. Observational errors

In order to estimate the uncertainty in the adopted TO magnitude, we used the same method as in Rosenberg et al. (1999). We built about one hundred synthetic CMDs for each cluster, using the isochrones by Pietrinferni et al. (2004). The synthetic CMDs were constructed by adopting for each cluster the corresponding metallicity, an age in the range between 10 and 13 Gyr, the photometric errors (as estimated from artificial star experiments), and the total number of stars in the observed CMD, and varying only the initial random number generator seed. The same procedure used to determine the TO in the observed CMD (see the explanation in the previous Section) was then applied to the synthetic diagrams. We estimated the error in the TO colour and magnitude in each observed CMD as the standard deviation of all the TOs measured in the corresponding synthetic diagrams.

This procedure does not take into account the effects due to differential reddening. Therefore the error estimated for clusters whose CMDs show this effect (namely NGC 4372, NGC 5927, NGC 6273, and NGC 6544) is likely to be underestimated. The error on the mean of the preliminary TO magnitudes for NGC 6273 (the worst case) is approximately a factor 2 larger than the error calculated from the synthetic diagrams. Nevertheless, we decided to adopt this technique for its reliability and for consistency with Rosenberg et al. (1999).

Regarding the errors on the ZAHB magnitude of the intermediate and metal poor clusters, they are dominated by the error in matching the HB of the template cluster with that of the object cluster, particularly for clusters with only a blue HB. As in Recio-Blanco et al. (2005), we repeated the fit many times, and estimated the error as the maximum difference between the single shift values and the final adopted one. This error estimate has been divided by 3, in order to have the

classical $1\text{-}\sigma$ value for a Gaussian distribution of the errors (in order to make it comparable with the errors of the TO magnitudes²). For the metal rich clusters, the main source of error is the uncertainty in the position of the lower envelope, particularly in clusters with a small number of stars.

In estimating errors in the vertical parameter, we considered the errors on the ZAHB and TO magnitudes to be independent, and thus summed in quadrature the two contributions.

2.4. The measured parameters

Table 2 lists the most relevant cluster parameters, including those measured in this paper, for the HST snapshot clusters. Col. 1 gives the cluster name; Col. 2 and 3 give the metallicity in the ZW and CG scale, respectively; Col. 4 gives the Galactocentric distance. Columns 5, 6 of Table 2 give the TO magnitudes and errors, respectively, in the $F555W$ band, while the $F555W$ ZAHB magnitudes and errors are in Col. 7, 8. Finally, Col. 9, 10 list the vertical parameter value, in the $F555W$ band, for the snapshot clusters. Table 3 provides the same quantities as Table 2, but for the groundbased clusters. The magnitudes of Table 3 are therefore in the V -band.

As already mentioned, we have used the same database (Rosenberg et al. 2000a,b) used by Rosenberg et al. (1999), but for consistency reasons we decided to re-measure the vertical parameter. Figure 3 shows the comparison between the TO and ZAHB magnitudes, and between the vertical parameters of the present study and those listed by Rosenberg et al. (1999) for the groundbased clusters. While the TO values are in very good agreement, there is some hint of a trend with the metallicity (though it is mostly within the average measurement errors) for the differences in ZAHB magnitudes in the intermediate and low metallicity range. This was expected because of the different method adopted in the two studies and the different definition of the ZAHB level. Rosenberg et al. (1999) used the same (empirical) template for all the intermediate and metal poor clusters. We think that the method used in the present paper is more reliable, as it is able to better account for the differences in the HB at varying the cluster metallicities.

3. Ages

3.1. The age determination

To measure the cluster relative ages, we compared our observed vertical parameters with the theoretical counterpart obtained from the set of α -enhanced isochrones of Cassisi et al. (2004), available in both the WFPC2/HST photometric bands, and the Johnson-Cousins system.

²Note that in Table 3 of Recio-Blanco et al. (2005) we list the maximum error.

For each isochrone, the theoretical TO was determined as the bluest point of the MS, and the ZAHB level was taken as the magnitude of the ZAHB model at $\log T_{\text{eff}} = 3.85$. We performed a 2-dimensional bicubic spline to set a finer grid in age and metallicity, and thus to give an estimate of the age for each cluster in the sample.

Figures 4 and 5 show the theoretical $\Delta F_{555W_{TO-HB}}$ and ΔV_{TO-HB} values as a function of $[\text{Fe}/\text{H}]$ for various ages, together with the observational points from the HST snapshot and groundbased observations, respectively. The upper panel of each figure adopts the ZW metallicity scale, whereas the lower panel refers to the CG scale. The two data sets are presented separately due to the different photometric systems.

Both Figures 4 and 5 show that the mean age of the metal poor clusters is about 1.5 Gyr older than the mean age of the clusters with $[\text{Fe}/\text{H}]_{\text{ZW}} > -1.7$ ($[\text{Fe}/\text{H}]_{\text{CG}} > -1.4$). At intermediate metallicities ($-1.7 < [\text{Fe}/\text{H}]_{\text{ZW}} < -0.8$), the age spread is increased by a group of a few clusters showing a younger age. This will be discussed further in the next Section.

Keeping in mind that the purpose of this work is to measure relative ages, and following Rosenberg et al. (1999), we calculated for each cluster a **normalised age**, defined as the ratio between the cluster age and the mean age of the group of metal poor clusters. More specifically, in case of the ZW metallicity, we used as normalising factor the mean age of the clusters with $[\text{Fe}/\text{H}]_{\text{ZW}} < -1.7$, i.e. 11.2 Gyr. For the CG metallicity scale, the normalising age is equal to 10.9 Gyr, corresponding to the mean age of the clusters with $[\text{Fe}/\text{H}]_{\text{CG}} < -1.4$. Columns 11–14 of Tables 2 and 3 give the estimated normalised ages and errors for the HST snapshot and the groundbased sample, respectively. In both tables, Col. 11, 12 give the normalised ages, and the corresponding errors adopting the ZW metallicity scale, and Col. 13, 14 the normalised ages and the corresponding errors for the CG metallicity scale.

As it can be inferred from the values in Tables 2 and 3, and as it will be discussed in Section 4, the group of clusters at intermediate metallicity shows a large age dispersion. We have verified that the age differences derived from the vertical parameter are indeed correct. In particular, we focussed our attention on a few clusters with nearly the same metallicity, within 0.1 dex, at $[\text{Fe}/\text{H}]_{\text{ZW}} \sim -1.3$. Some of these clusters have been the subject of a long and lively discussion in the literature in the last 10 years or so (e.g. Stetson et al. 1996; Sandquist et al. 1996; VandenBerg 2000) in the attempt to establish whether they are coeval or not. According to the vertical parameter, NGC 362, NGC 1261, NGC 1851, NGC 2808, NGC 5904 have all the same age, within the uncertainties (5–8%), and are 10–15% younger than another group of older (and coeval among them) clusters which includes NGC 288, NGC 5946, NGC 6218, NGC 6121, NGC 6266, NGC 6362, NGC 6717. In order to check this observational evidence, in Figures 6 and 7 we directly compare the HB population and the fiducial points reproducing the location of the main sequence and sub-giant branch (SGB) of the CMDs of four couples of clusters selected among the above mentioned objects. The HB stars and the fiducial points have been shifted in magnitude in order to have the TO point at magnitude 0. One of the two clusters has been shifted in colour by the amount required to take the

TOs at the same colour. Figure 6 shows this comparison for two couples of nearly coeval clusters (NGC 362 - NGC 1261 and NGC 362 - NGC 1851): all the sequences match remarkably well, and it is hard to infer any age difference among these objects. These clusters were also found to be nearly coeval by Sandquist et al. (1996) and Vandenberg (2000). Figure 7 compares two of these young clusters (NGC 362 and NGC 1851) with NGC 6121, which results older: despite the TO and SGB regions match well, the HB levels significantly differ, as expected from our vertical parameters. The difference in magnitude between the HB levels is indicative of the different ages.

3.2. Comparison between the two catalogues

The homogeneity of the observational database is a crucial ingredient for accurate relative age measurement. In this paper, we use two catalogues of CMDs coming from rather different observational systems, with similar, but not identical bandpasses. This means that we cannot directly compare the parameters obtained from the empirical CMDs. Even if the models used for the age determination have been appropriately transformed into the two observational systems before comparison with the observed parameters, it is important to verify that the ages coming from the two data sets are mutually consistent. For this reason, we took advantage of the 16 clusters in common between the HST snapshot and the groundbased data set. Figure 8 shows the difference between the ages from the snapshot and the groundbased catalogues for the common clusters. The average difference is consistent with zero, and there is no trend with the cluster metal content. Figure 8 tells us that we can merge the two age catalogues, and use them together in analysing the relative ages of the Galactic globular clusters.

3.3. Comparison with other models

Comparison with stellar models is critical for any cluster age determination. In principle, differences in the input physics (i.e. equation of state, opacities) input parameters (i.e. the helium enrichment ratio $\Delta Y/\Delta Z$) and transformations from the theoretical to the observational plane, may have a significant impact on the final ages and the inferred star formation history of the Galactic GC system.

To assess the consistency of our relative age determination, at least within the recent theoretical framework, we compared in Fig. 9 our normalised ages for the groundbased sample with the values estimated using the two isochrone sets already employed by Rosenberg et al. (1999), i.e. the Straniero, Chieffi, & Limongi (1997) and Bergbusch & Vandenberg (2001) isochrones calculated by interpolating the evolutionary tracks by Vandenberg et al. (2000). Apart from the heavy element mixture, these two sets of isochrones differ from our reference models mainly with respect to the adopted equation of state, bolometric corrections, and helium abundance at a given metallicity. About this latter point, the models by Straniero et al. (1997) use $Y = 0.23$, whereas Vandenberg

et al. (2000) employ $Y = 0.235 + 2Z$, and Cassisi et al. (2004) make use of $Y = 0.245 + 1.4Z$. It is worth noticing that the initial He abundance (Y) adopted in the stellar computation has a strong effect on both the core H-burning lifetime and on the HB luminosity level. More in details, for a fixed age, when the value of Y increases, the TO of the isochrone becomes fainter, whereas the HB luminosity level increases. As a consequence the value of the ΔV_{TO-HB} parameter increases. So for a fixed age, the adopted Helium-enrichment ratio, affects the trend of the ΔV_{TO-HB} parameter with Z . The net effect on the age estimate is to make a cluster of a given metallicity younger when He increases. Therefore, an increase of the Helium-enrichment ratio enhances, if present, any age-metallicity relationship (in the sense of making the more metal rich clusters younger in comparison with the more metal poor ones).

Given that VandenBerg et al. (2000) models include a larger Helium enrichment ratio with respect to Cassisi et al. (2004), we expect that their use produces younger relative ages for the more metal rich clusters. The different Helium-enrichment ratio is also the main reason for the different behaviours of the ΔV_{TO-HB} parameter with the metallicity at a fixed age.

In addition, the Straniero et al. (1997) models account for Helium diffusion, which is neglected in the other isochrone sets.

When deriving the theoretical ΔV_{TO-HB} -age-[Fe/H] calibration from the Straniero et al. (1997) scaled solar isochrones, we used the property that the ΔV_{TO-HB} values at a given age are to a good approximation the same for both a scaled solar metal distribution and an α -enhanced one typical of GCs (see, e.g. Salaris, Chieffi, & Straniero 1993; VandenBerg et al. 2000; Cassisi et al. 2004) with the same metal mass fraction Z , at least for metal poor objects. Bearing in mind that the relation between global metallicity [M/H] and [Fe/H] is different for α -element enhanced mixtures, the ΔV_{TO-HB} -age-[M/H] calibration obtained in this way was then transformed to a ΔV_{TO-HB} -age-[Fe/H] relationship using $[M/H] = [Fe/H] + 0.3$, which is appropriate for $[\alpha/Fe] = +0.4$.

The comparison of the normalised ages discloses very good agreement for $[Fe/H]_{ZW} < -1.9$. Moving towards higher [Fe/H] our ages become increasingly younger up to $[Fe/H]_{ZW} \sim -1.1$. The maximum difference with the VandenBerg et al. (2000) and Straniero et al. (1997) models is $\sim 5\%$ and $\sim 8\%$, respectively, of the same order of magnitude as the error bars due to the observational uncertainties. For more metal rich clusters the difference decreases to $\sim 5\%$ for the Straniero et al. (1997) models, whereas the difference between our ages and those obtained using the VandenBerg et al. (2000) models seems to be reversed, with the VandenBerg et al. (2000) ages younger than ours by $\sim 5\%$ for the three clusters at $[Fe/H] \sim -0.6$.

We have also compared our normalised ages with the results obtained using the Girardi et al. (2000) models. In this case, there is generally a better agreement between the two age sets, with some differences (always smaller than 5%) at the two extremes of the metallicity interval covered by our data set.

Despite these discrepancies, for the purposes of this paper, the comparisons in Fig. 9 show that there is a substantial agreement among the ages obtained with recent stellar evolution models:

the overall picture of the age distribution discussed in the next Section would not change if we were to consider the normalised ages obtained from the VandenBerg et al. (2000), Straniero et al. (1997) or Girardi et al. (2000) models. It is the size of the trends of the average normalised ages with metallicity that would marginally change, although an agreement at the level of $\sim 5 - 8\%$ (comparable with the observational errors) among rather different model sets is encouraging. By contrast the trend of the age dispersion with metallicity is more solid, as it mainly depends on the dispersion of the observed parameters, and much less (and in any case much less than the observational errors) on the adopted models.

4. Discussion

Figures 10 and 11 plot the normalised ages as a function of the metallicity, and of the distance from the Galactic centre for the two adopted metallicity scales. Different symbols represent the different metallicity ranges listed in the figure caption. Open symbols represent the HST snapshot data, whereas filled symbols are for the groundbased clusters. For the clusters in common between the two catalogues, we plot the age obtained from the vertical parameter measured on the HST snapshot CMDs. The dashed line represents the zero point: clusters with a normalised age equal to 1, have an age of 11.2 Gyr and 10.9 Gyr for the ZW and CG metallicity scales, respectively. The overall trend already displayed by Figures 4 and 5 is more easily visible in Figures 10 and 11: the most metal poor clusters ($[\text{Fe}/\text{H}]_{\text{ZW}} < -1.7$, $[\text{Fe}/\text{H}]_{\text{CG}} < -1.4$) are all older, and coeval, with an age dispersion smaller than 0.6 Gyr, which is compatible with a null age dispersion, if we take into account the measurement errors. The clusters with $-1.7 < [\text{Fe}/\text{H}]_{\text{ZW}} < -0.8$ ($-1.4 < [\text{Fe}/\text{H}]_{\text{CG}} < -0.8$) are, on average, 1.5 Gyr³ younger, and show a larger age dispersion (1.0 Gyr), with an age total range of ~ 3 Gyr. Interestingly enough, 15% (5 out of 32) of the clusters in this metallicity interval seems to be coeval with the most metal poor ones. The age dispersion is independent of the adopted stellar evolution model. More metal rich clusters have on average the same age as the intermediate metallicity ones, but apparently with a smaller age dispersion, though the small number of objects and the differences in the ages from the different model sets (cf. Fig 9) do not allow any firm conclusion for this group of clusters. There is no evidence for a dependence of age on the distance from the Galactic centre, though all the clusters with $R_{\text{GC}} > 20$ kpc are old (but these are all metal poor clusters).

In the following we consider a few peculiar objects. On average, we note that the metal poor clusters are the oldest clusters. However, among them, two clusters (NGC 4590 and NGC 7078) seem to be about 8% younger. Interestingly enough, Yoon & Lee (2002) listed these two GCs among a group of low-metallicity clusters that display a planar alignment in the outer halo, probably the consequence of an accretion event from a Galactic satellite system. On the other hand, in the same

³This number would remain the same using the Girardi et al. (2000) isochrones, but it should be reduced to about 1.0 and 0.7 Gyr respectively, if the models of VandenBerg et al. (2000) and Straniero et al. (1997) are adopted.

paper also NGC 7099 and NGC 5024 are indicated as members of the same group, while in our study they seem to be coeval with the remaining metal poor clusters.

There are a few intermediate metallicity clusters that show a much younger age, namely NGC 362 (the youngest of the whole sample, with an age 27% younger than the zero relative age level), NGC 1261, NGC 2808, NGC 3201 and NGC 1851. All these clusters were already known to be younger objects (Rosenberg et al. 1999). Figure 1 in Fusi Pecci et al. (1995) displays the position of some galactic clusters in galactocentric coordinates indicating the position of two planes passing in the vicinity of some satellite galaxies of the Milky Way. NGC 1261, NGC 2808 and NGC 1851 are located very close to the Fornax-Leo-Sculptor plane. The galactocentric coordinates of NGC 362 and NGC 3201 can be calculated starting from the galactic coordinates (l, b) , and the distance from the galactic centre (Harris 1996, in the revised version of 2003): both clusters are found to be very close to the same plane.

None of the clusters suspected of being members of the Sagittarius Stream (Bellazzini, Ferraro, & Ibata 2003), and present in our catalogue (NGC 288, NGC 4147, NGC 5053, NGC 5466, NGC 5634, NGC 7089), seems to be significantly younger than the average of the other clusters with similar metallicity, though it is well established that other clusters of the same stream are definitely young, e.g. Pal 12 (Rosenberg et al. 1998), Ruprecht 106 (Buonanno et al. 1990), Terzan 7 (Buonanno et al. 1995b).

5. Conclusions

We presented a catalogue of homogeneous, relative ages obtained from the so called vertical parameter for a sample of Galactic GCs.

The analysis of the relative age distribution gives some hints on the origin of the GC system of our Galaxy. In particular, we have shown that the low metallicity clusters ($[\text{Fe}/\text{H}] \leq -1.7$) are the oldest GCs. The low metallicity clusters show a very small age dispersion (< 0.6 Gyr), compatible with a null age dispersion, if we account for the measurement errors. Among the low-metallicity clusters, there are a couple of objects which are marginally younger. These objects are part of a suspected Galactic stream, which might indicate accretion from outside the Galaxy, or debris from the tidal disruption of a Galactic satellite.

The clusters at intermediate metallicities ($-1.7 \leq [\text{Fe}/\text{H}]_{\text{ZW}} \leq -0.9$) are up to 3 Gyr younger than the more metal poor ones, with an age dispersion of ~ 1.0 Gyr. A small sample of objects (15%) seems to be coeval with the most metal poor GCs. It must be explicitly noted that, while the age dispersion seems to be a solid result, the dependence of the *mean* age on metallicity and its value are model dependent. The empirical facts outlined above imply that most of the GCs with $[\text{Fe}/\text{H}]_{\text{ZW}} \geq -1.7$ were born between 0.5 and 1 Gyr after a first generation of more metal poor clusters. A few of the intermediate metallicity clusters are up to 3 Gyr younger than the oldest clusters in the same metallicity range and this last result is not model dependent. Interestingly

enough, all these young clusters seem to be related to some Galactic streams, i.e. linked to some tidal disruption event (of an external object or a smaller satellite), though these streams contain also some of the oldest known GCs.

Finally, all the metal rich clusters are at least 1 Gyr younger than the most metal poor ones, with a relatively small age dispersion. The metal rich sample is still too poor, however, to enable firmer conclusions to be reached.

We do not see any correlation of the cluster ages with the Galactocentric distance. However, all the clusters with Galactocentric distances greater than 20 kpc are old, with a very small age dispersion. These clusters are also in the metal poor sample.

In concluding this paper, it is worth adding a final remark. Other parameters, as Helium variations, $[\alpha/\text{Fe}]$ differences, cluster to cluster deep mixing (due to internal rotation) affect the vertical separation between the TO and the ZAHB. We have already commented the effect of He-enrichment as a function of metallicity in Section 3.3. Here, we note that there is no evidence of significant cluster to cluster He variations, as shown by Salaris et al. (2004) using our snapshot database. However, recent results on the massive clusters ω Centauri (Bedin et al. 2004, Piotto et al. 2005) and NGC 2808 (D’Antona & Caloi 2004) indicates that within the same cluster, there could be two generations of stars, with the second generation being Helium enriched. If this occurrence is confirmed, and if the same scenario is present also in less massive clusters, the ages derived from the vertical parameter could be affected. As for the other parameters, we plotted our relative ages as a function of $[\alpha/\text{Fe}]$ for the clusters for which this parameter has been measured, and we did not find any correlation. The effect of deep mixing variations is at the moment impossible to assess from the observational point of view. In conclusion, the main parameter able to explain our measured vertical parameter variations, at least inside the metallicity bins of Figures 10 and 11 is still age.

We warmly thank A.R. Walker and E. Sandquist for providing us their data for some clusters. We also thank Douglas C. Heggie for a careful reading of the manuscript, and the anonymous referee for useful comments. GP, SC acknowledge partial support from the Ministero dell’Istruzione, Università e Ricerca (*MIUR*, PRIN2002, PRIN2003), and from the Agenzia Spaziale Italiana (*ASI*).

REFERENCES

- Bellazzini, M., Ferraro, F. R., & Ibata, R. 2003, *AJ*, 125, 188
- Bedin, L. R., Piotto, G., Anderson, J., Cassisi, S., King, I. R., Momany, Y., & Carraro, G. 2004, *ApJ*, 605, L125
- Bergbusch, P. A., & Vandenberg, D. A. 2001, *ApJ*, 556, 322
- Buonanno, R., Corsi, C. E., Pulone, L., Fusi Pecci, F., & Bellazzini, M. 1998, *A&A*, 333, 505

- Buonanno, R., Corsi, C. E., Pecci, F. F., Richer, H. B., & Fahlman, G. G. 1995a, *AJ*, 109, 650
- Buonanno, R., Corsi, C. E., Pulone, L., Pecci, F. F., Richer, H. B., & Fahlman, G. C. 1995b, *AJ*, 109, 663
- Buonanno, R., Buscema, G., Fusi Pecci, F., Richer, H. B., & Fahlman, G. G. 1990, *AJ*, 100, 1811
- Carretta, E., Cohen, J. G., Gratton, R. G., & Behr, B. B. 2001, *AJ*, 122, 1469
- Carretta, E. & Gratton, R. G. 1997, *A&AS*, 121, 95
- Cassisi, S. & Salaris, M. 1997, *MNRAS*, 285, 593
- Cassisi, S., Salaris, M., Castelli, F., & Pietrinferni, A. 2004, *ApJ*, astro-ph/0408111
- Chaboyer, B., Demarque, P., Kernan, P. J., & Krauss, L. M. 1998, *ApJ*, 494, 96
- D’Antona, F., & Caloi, V. 2004, *ApJ*, 611, 871
- Fusi Pecci, F., Bellazzini, M., Cacciari, C., & Ferraro, F. R. 1995, *AJ*, 110, 1664
- Girardi, L., Bressan, A., Bertelli, G., & Chiosi, C. 2000, *A&AS*, 141, 371
- Gratton, R. G., Bragaglia, A., Carretta, E., Clementini, G., Desidera, S., Grundahl, F., & Lucatello, S. 2003, *A&A*, 408, 529
- Harris, W. E. 1996, *AJ*, 112, 1487
- Hoyle, F. & Schwarzschild, M. 1955, *ApJS*, 2, 1
- Pietrinferni, A., Cassisi, S., Salaris, M., & Castelli, F. 2004, *ApJ*, 612, 168
- Piotto, G., et al. 2002, *A&A*, 391, 945
- Piotto, G., et al. 2005, *ApJ*, astro-ph/0412016
- Recio-Blanco, A., et al. 2005, *A&A*, astro-ph/0408462
- Renzini, A. & Fusi Pecci, F. 1988, *ARA&A*, 26, 199
- Riello, M., et al. 2003, *A&A*, 410, 553
- Rosenberg, A., Aparicio, A., Saviane, I., & Piotto, G. 2000a, *A&AS*, 145, 451
- Rosenberg, A., Piotto, G., Saviane, I., & Aparicio, A. 2000b, *A&AS*, 144, 5
- Rosenberg, A., Saviane, I., Piotto, G., & Aparicio, A. 1999, *AJ*, 118, 2306
- Rosenberg, A., Saviane, I., Piotto, G., & Held, E. V. 1998, *A&A*, 339, 61

- Rutledge, G. A., Hesser, J. E., Stetson, P. B., Mateo, M., Simard, L., Bolte, M., Friel, E. D., & Copin, Y. 1997, *PASP*, 109, 883
- Salaris, M., Riello, M., Cassisi, S., & Piotto, G. 2004, *A&A*, 420, 911
- Salaris, M. & Weiss, A. 2002, *A&A*, 388, 492
- Salaris, M. & Weiss, A. 1998, *A&A*, 335, 943
- Salaris, M., Chieffi, A., & Straniero, O. 1993, *ApJ*, 414, 580
- Sandage, A. R. & Schwarzschild, M. 1952, *ApJ*, 116, 463
- Sandquist, E. L., Bolte, M., Stetson, P. B., & Hesser, J. E. 1996, *ApJ*, 470, 910
- Sarajedini, A., Chaboyer, B., & Demarque, P. 1997, *PASP*, 109, 1321
- Stetson, P. B., Vandenberg, D. A., & Bolte, M. 1996, *PASP*, 108, 560
- Straniero, O., Chieffi, A., & Limongi, M. 1997, *ApJ*, 490, 425
- VandenBerg, D. A. 2000, *ApJS*, 129, 315
- VandenBerg, D. A., Swenson, F. J., Rogers, F. J., Iglesias, C. A., & Alexander, D. R. 2000, *ApJ*, 532, 430
- Walker, A. R. 1994, *AJ*, 108, 555
- Walker, A. R. 1998, *AJ*, 116, 220
- Yoon, S. & Lee, Y. 2002, *Science*, 297, 578
- Zinn, R. & West, M. J. 1984, *ApJS*, 55, 45

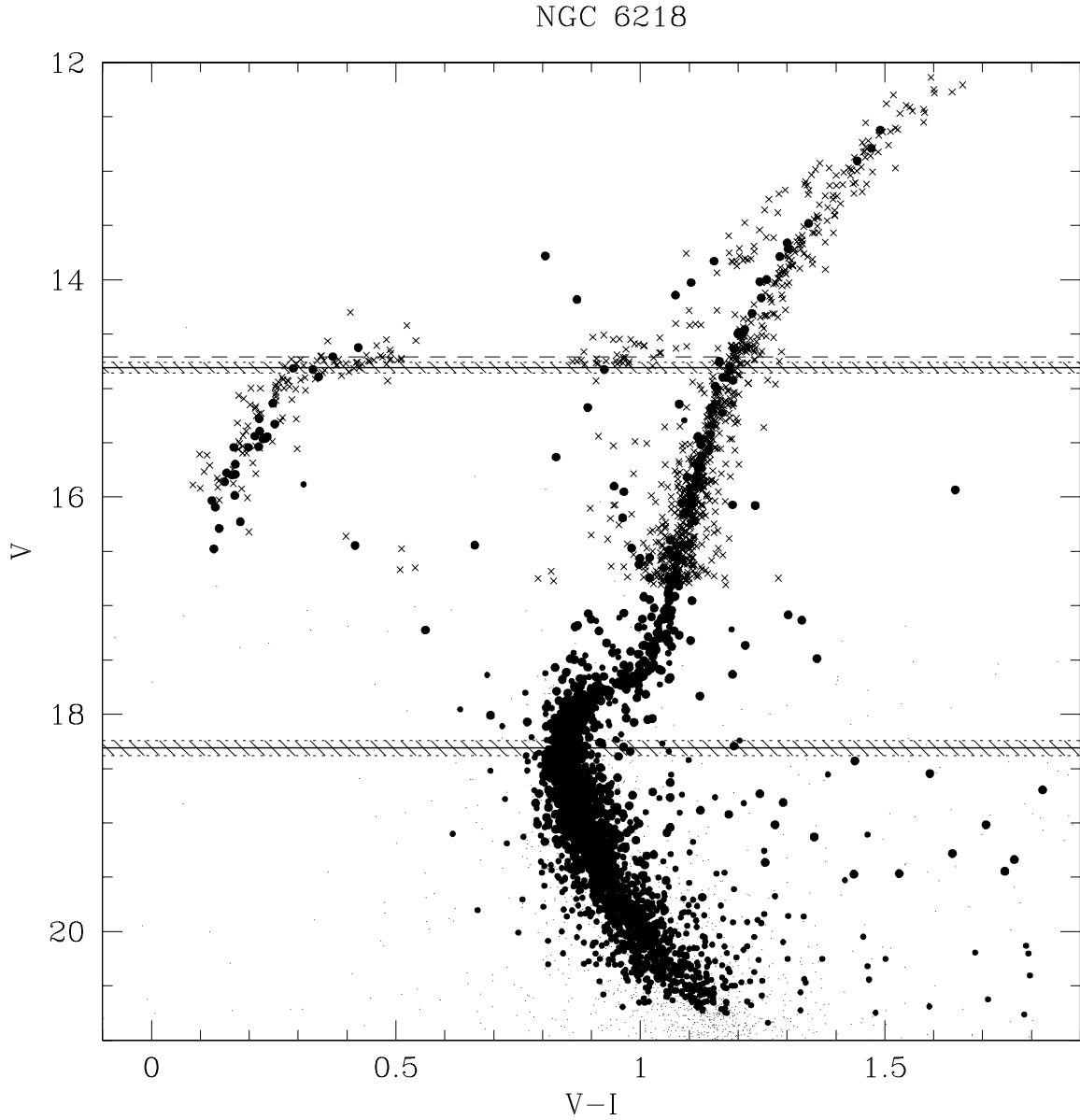


Fig. 1.— Groundbased CMD of the cluster NGC 6218 (dots). The crosses are the brighter section of the CMD of NGC 5904, the template used in the ZAHB measurements in the metallicity range of NGC 6218. The horizontal solid lines are the TO and ZAHB magnitudes. The dashed regions represent the $1\text{-}\sigma$ uncertainties. The dashed line is the RR Lyrae mean magnitude of the template cluster.

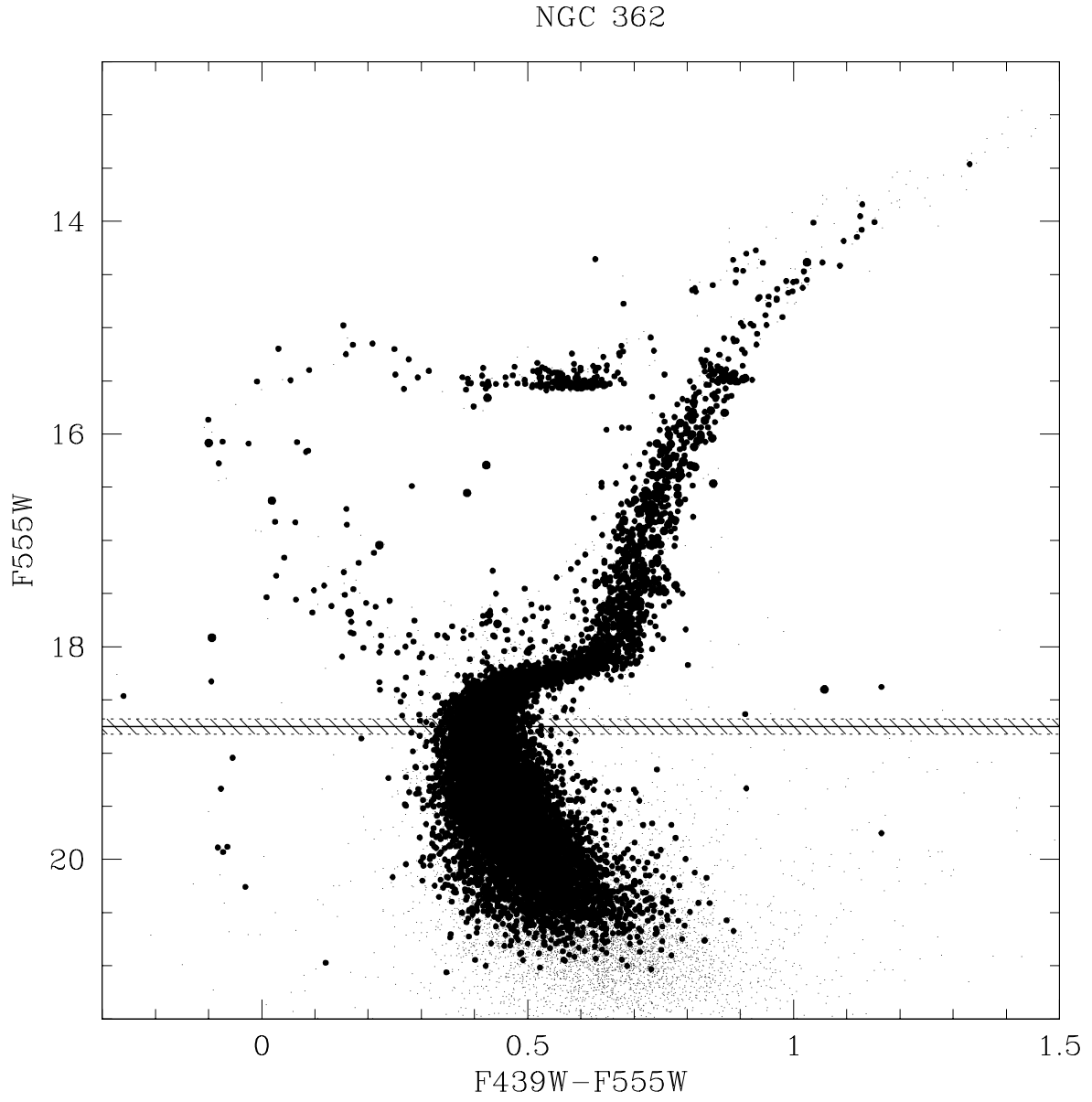


Fig. 2.— HST snapshot CMD of the cluster NGC 362. The horizontal solid line corresponds to the TO magnitudes. The dashed region represents the $1\text{-}\sigma$ uncertainty.

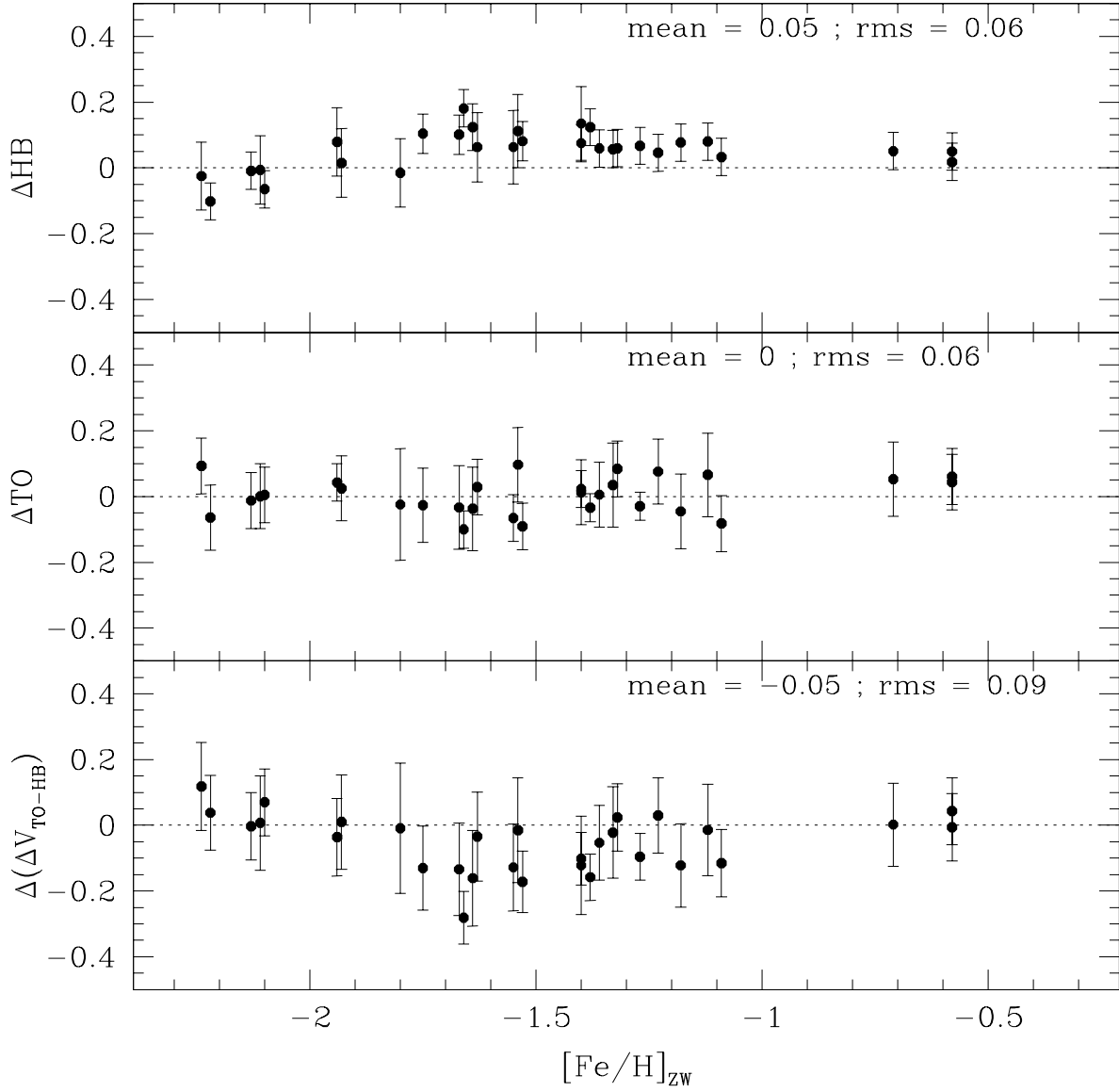


Fig. 3.— Comparison between our ZAHB (*upper panel*) and TO (*middle panel*) magnitudes and those listed by Rosenberg et al. (1999). The *lower panel* shows the corresponding differences in the vertical parameters.

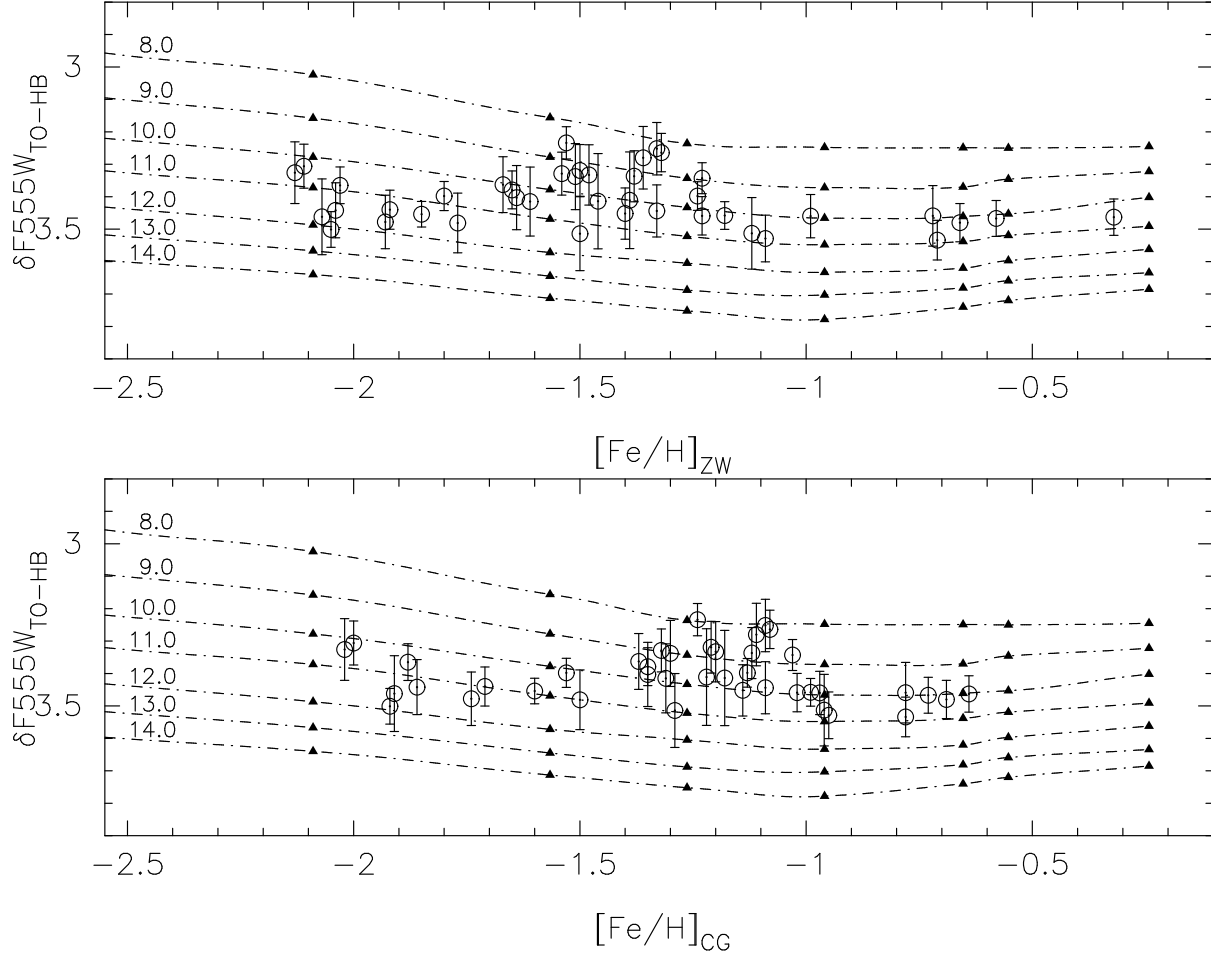


Fig. 4.— The vertical parameters measured on the HST snapshot cluster CMDs are plotted versus the metallicity (adopting the ZW scale in the *upper panel* and the CG one in the *lower panel*). The dashed lines show the theoretical predictions. The isochrones are spaced by 1 Gyr (starting from 14.0 Gyr at the bottom).

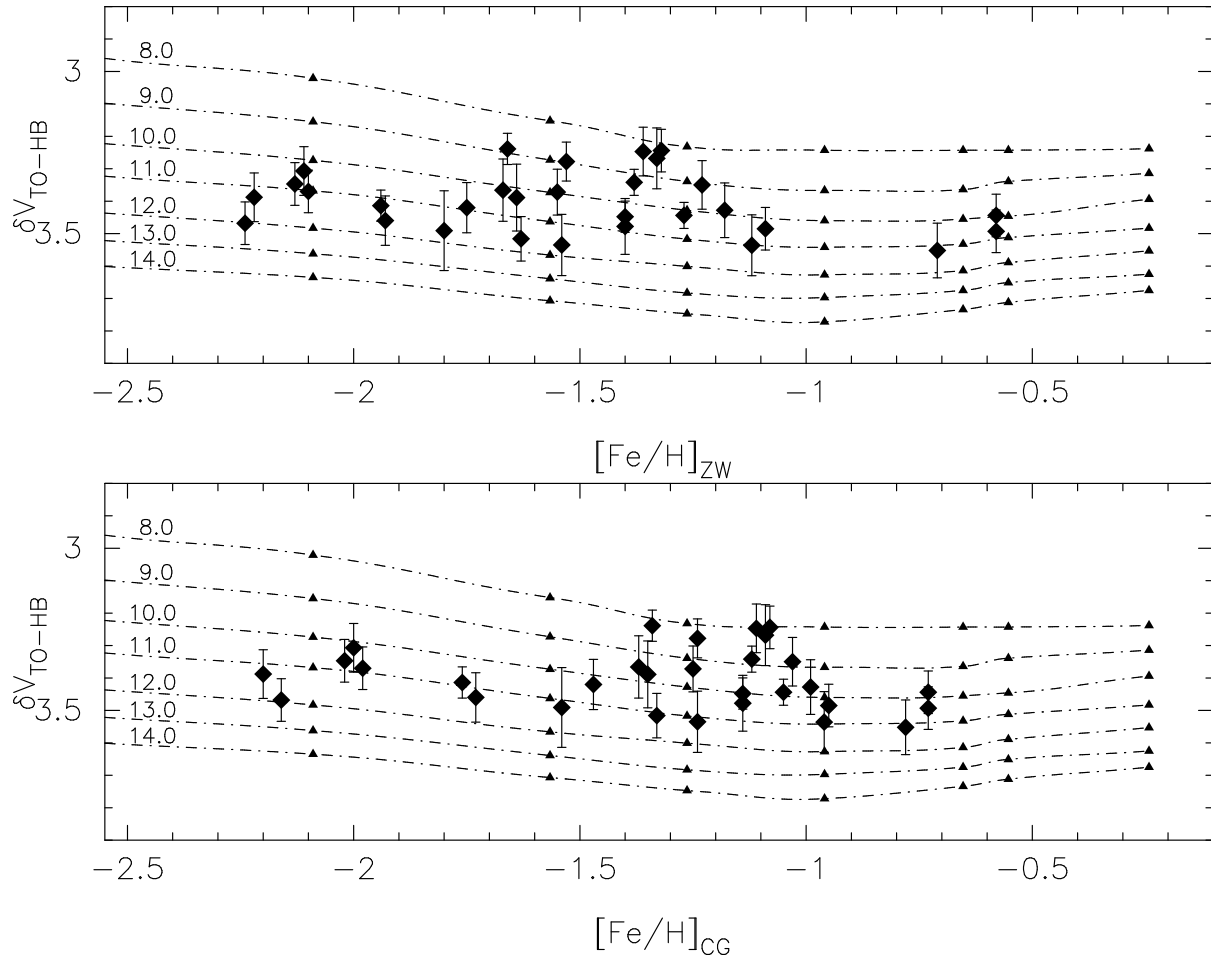


Fig. 5.— As in Fig. 4 for the groundbased sample.

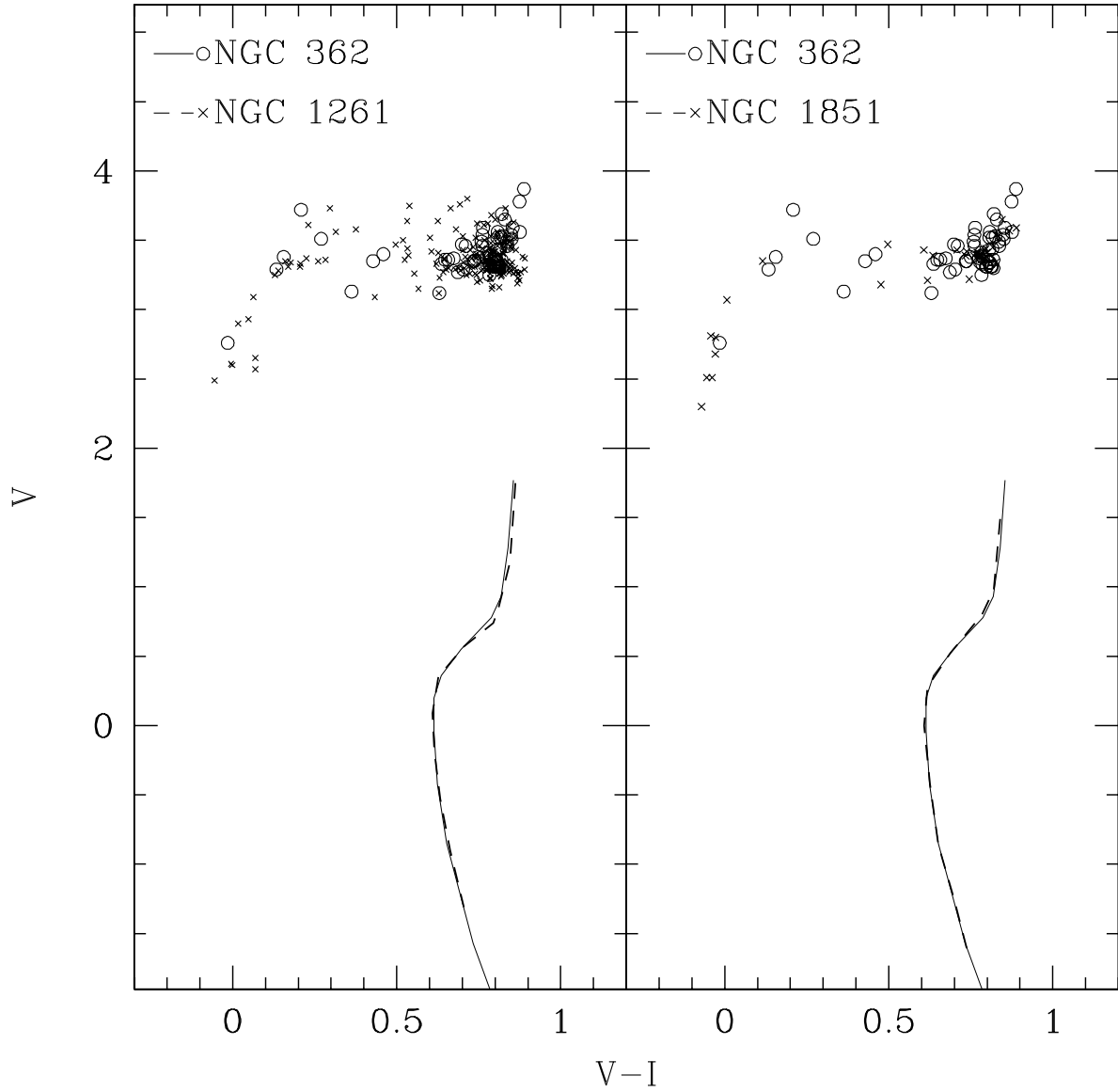


Fig. 6.— Comparison between the HB populations and the fiducial points reproducing the location of the main sequence and SGB of the CMDs of two couples of nearly coeval clusters: NGC 362 - NGC 1261 (*left panel*) and NGC 362 - NGC 1851 (*right panel*). The HB stars and the fiducial points have been shifted in order to match the positions of the TOs.

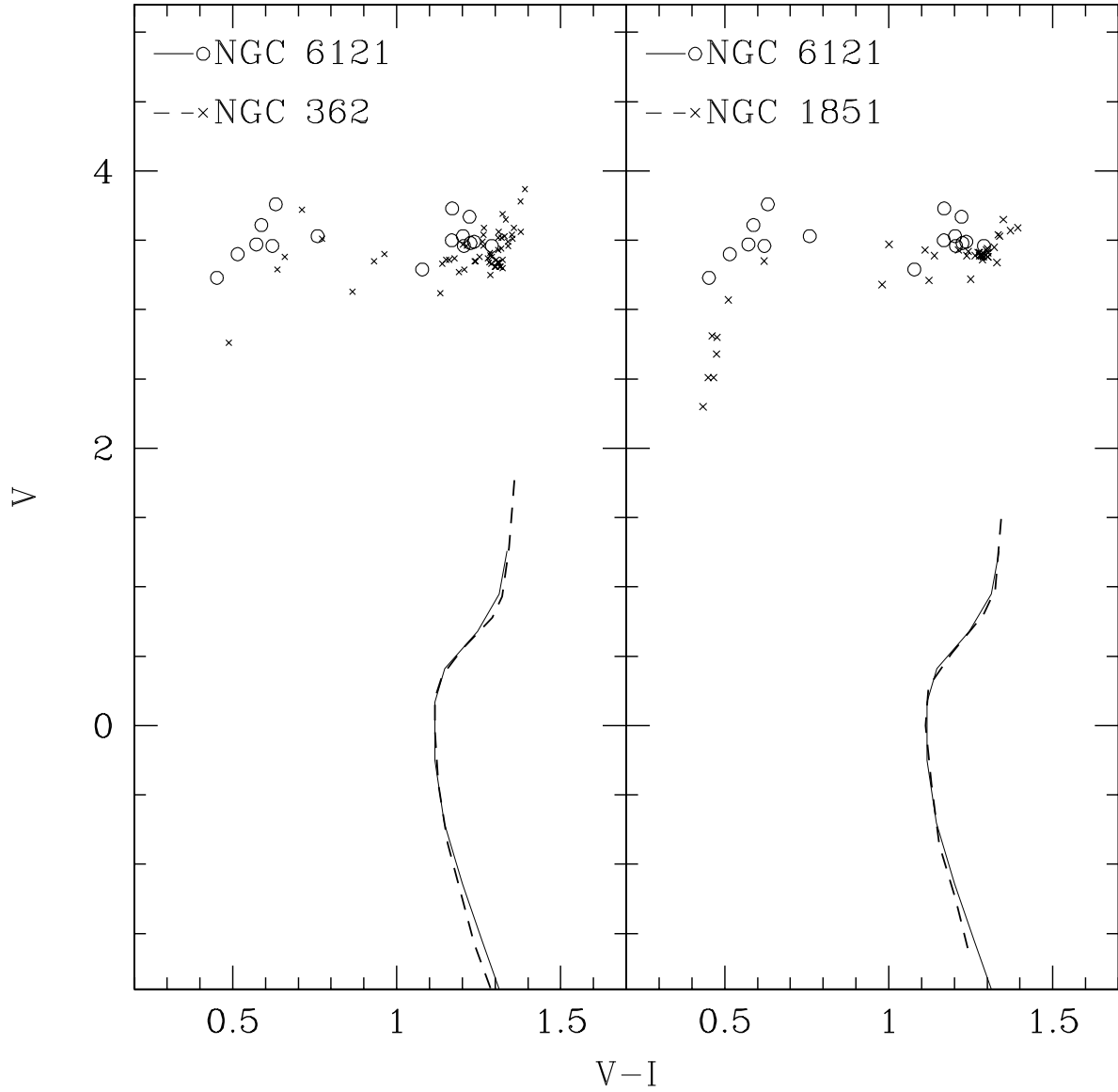


Fig. 7.— Comparison between the HB populations and the fiducial points reproducing the location of the main sequence and SGB of the CMDs of two young and nearly coeval clusters (NGC 362 and NGC 1851, *left* and *right panel* respectively) with the older NGC 6121. The HB stars and the fiducial points have been shifted in order to match the positions of the TOs.

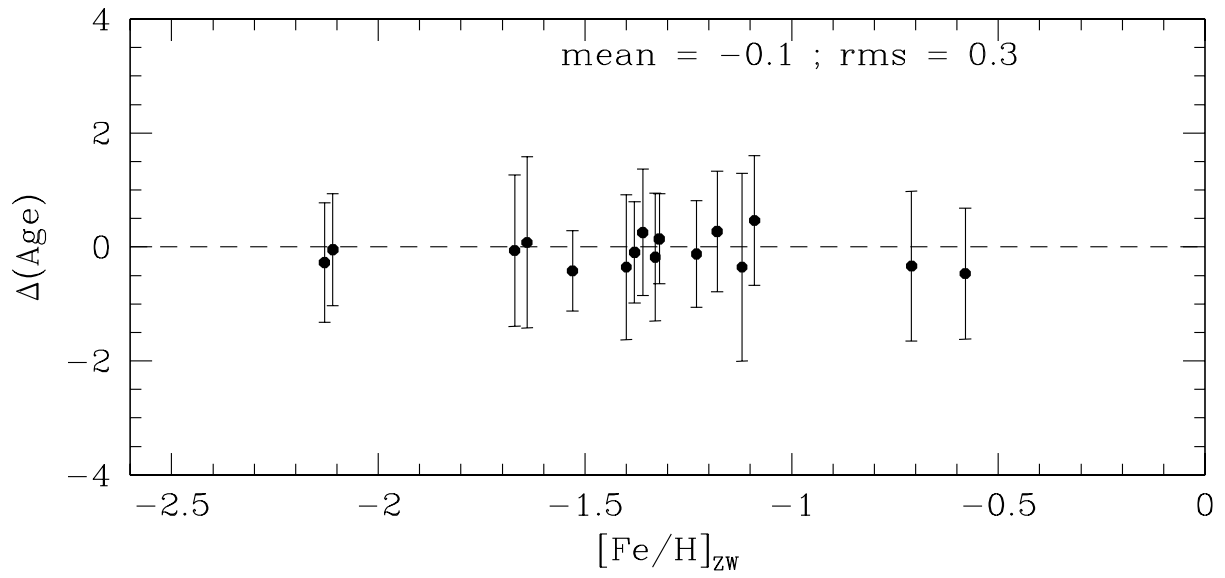


Fig. 8.— The age difference (in Gyr) from the two observational catalogues for the 16 GCs in common.

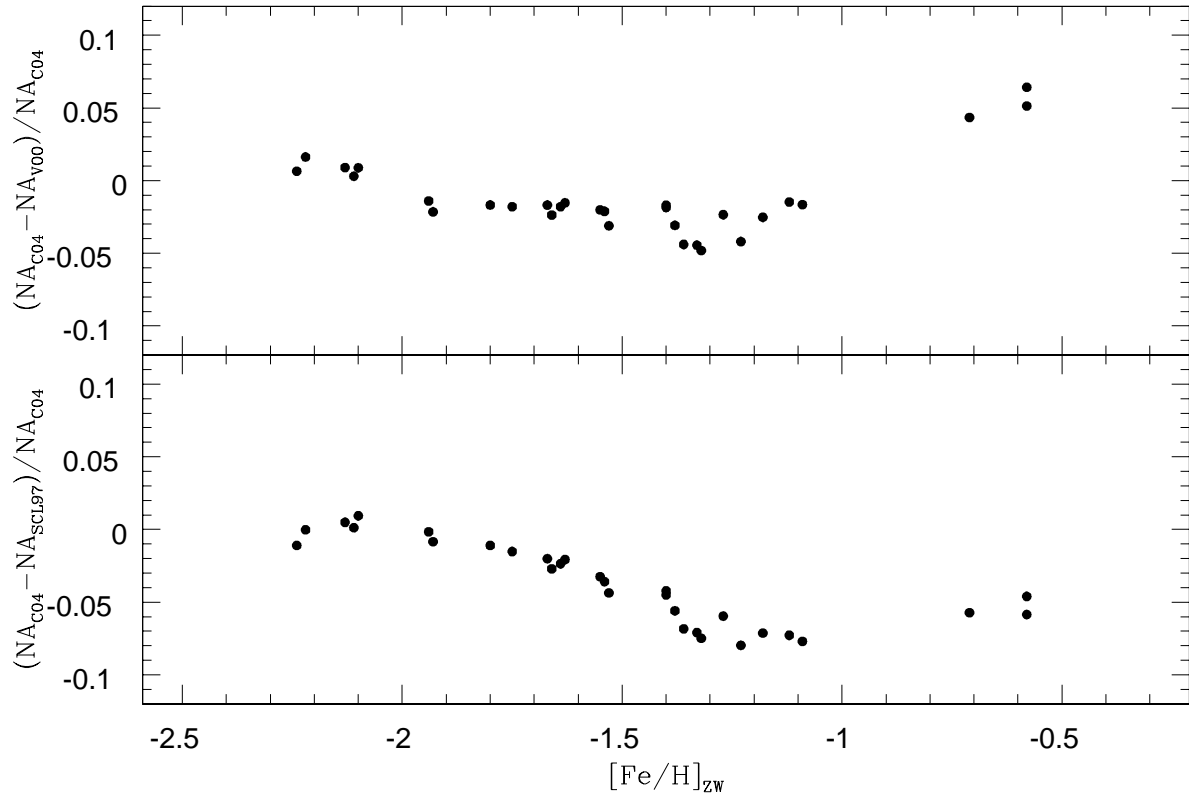


Fig. 9.— Comparison of the normalised ages (NA) estimated using three different model databases. C04, SCL97 and V00 denote, respectively, the Cassisi et al. (2004), Straniero et al. (1997) and Vandenberg et al. (2000) models.

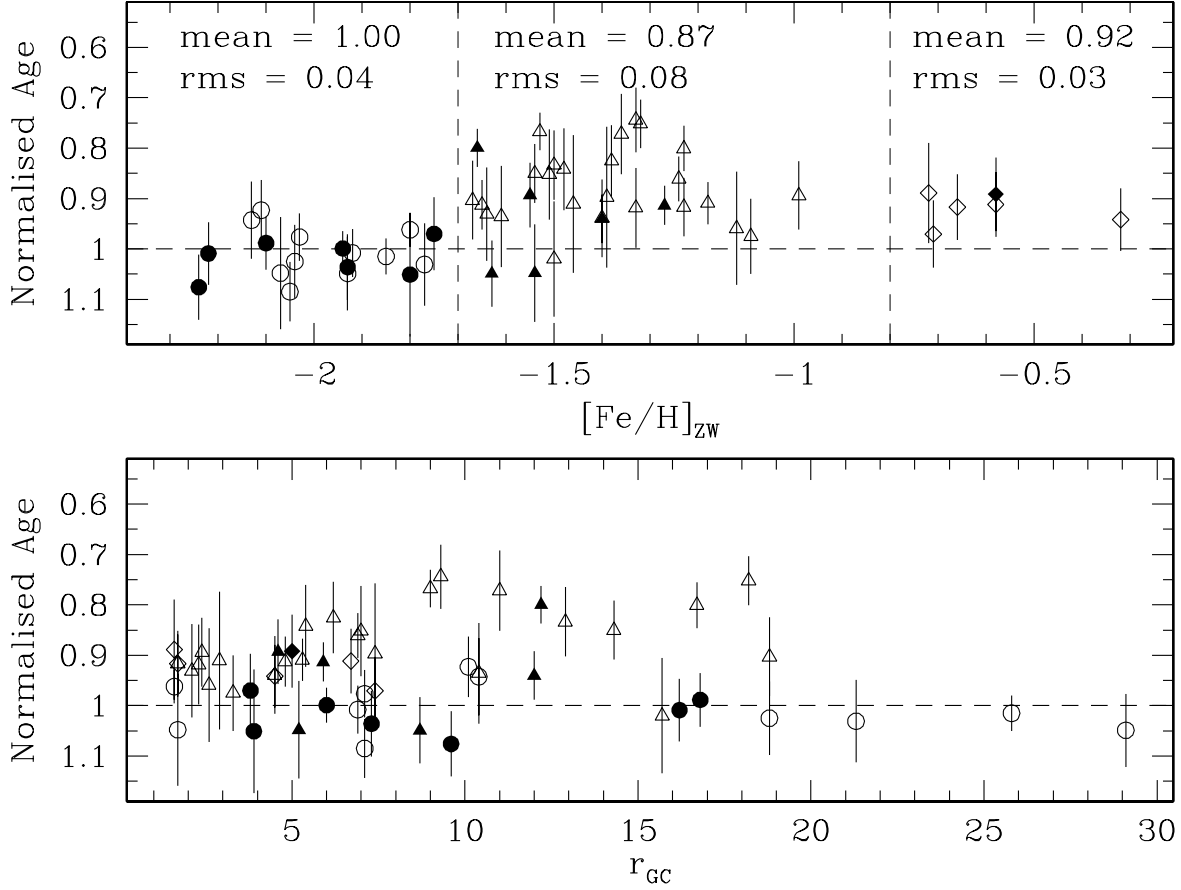


Fig. 10.— The normalised ages are plotted against the ZW metallicity (*upper panel*), and against the distance from the Galactic centre (*lower panel*). Filled symbols are for groundbased data and open symbols are for HST snapshot data. Circles refer to clusters with $[\text{Fe}/\text{H}]_{\text{ZW}} \leq -1.7$; triangles to clusters with $-1.7 < [\text{Fe}/\text{H}]_{\text{ZW}} < -0.8$, and diamonds to clusters with $[\text{Fe}/\text{H}]_{\text{ZW}} \geq -0.8$.

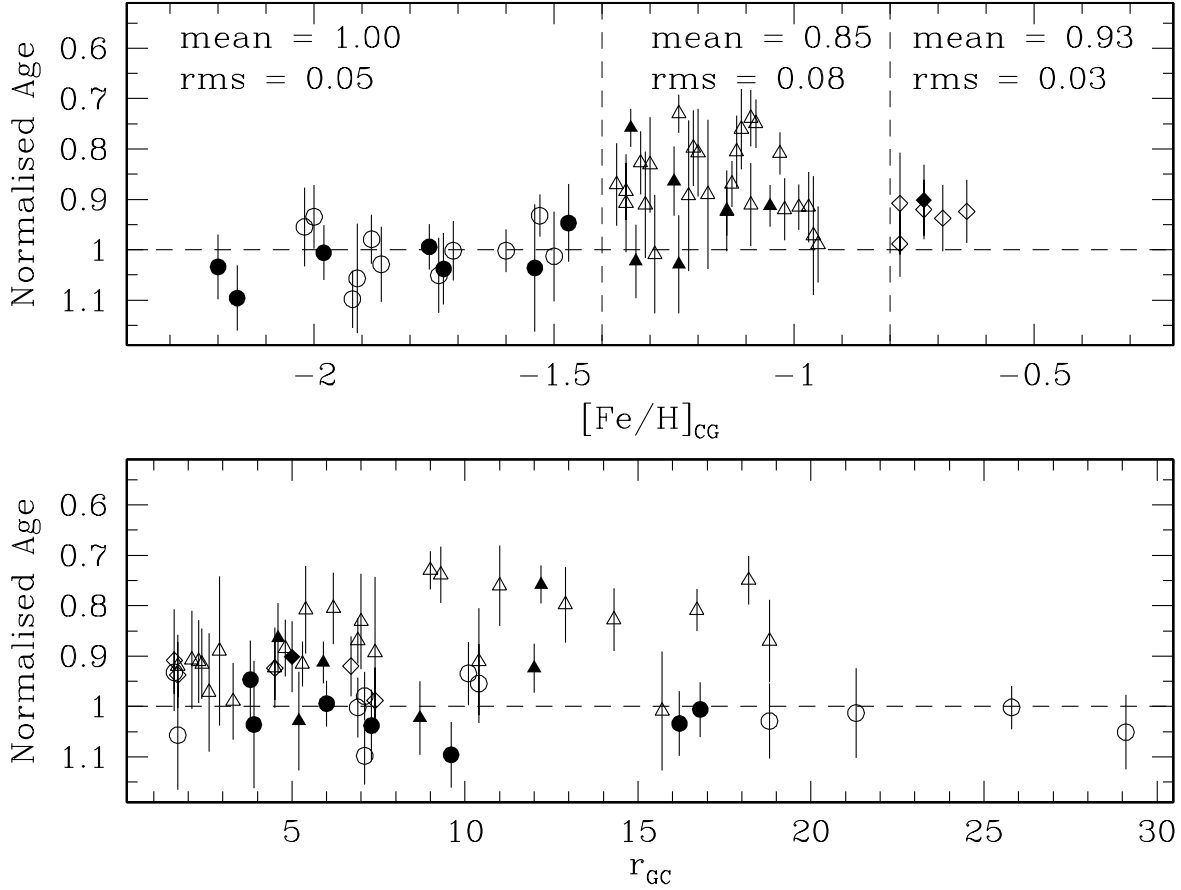


Fig. 11.— As in Fig. 10, but adopting the CG metallicity scale. Circles refer to clusters with $[\text{Fe}/\text{H}]_{\text{CG}} \leq -1.4$; triangles to clusters with $-1.4 < [\text{Fe}/\text{H}]_{\text{CG}} < -0.8$, and diamonds to clusters with $[\text{Fe}/\text{H}]_{\text{CG}} \geq -0.8$.

Table 1: Templates for the ZAHB measurement on groundbased clusters.

ID	Metallicity Interval	CMD Source
NGC 4590	$-2.3 \leq [\text{Fe}/\text{H}] \leq -1.8$	Walker (1994)
NGC 5272	$-1.8 \leq [\text{Fe}/\text{H}] \leq -1.5$	Rosenberg et al. (2000a)
NGC 5904	$-1.5 \leq [\text{Fe}/\text{H}] \leq -1.3$	Sandquist (priv. comm.)
NGC 1851	$-1.3 \leq [\text{Fe}/\text{H}] \leq -1.1$	Walker (1998)
NGC 6362	$-1.1 \leq [\text{Fe}/\text{H}] \leq -0.3$	Walker (priv. comm.)

Table 2. Observational parameters and normalised ages for the HST snapshot data. Clusters marked with an asterisk show differential reddening in their CMDs.

ID (1)	[Fe/H] _{ZW} (2)	[Fe/H] _{CG} (3)	r_{GC} (4)	$(F555W)_{TO} \pm \sigma$ (5)	$(F555W)_{HB} \pm \sigma$ (6)	$(F555W)_{HB} \pm \sigma$ (7)	$(F555W)_{HB} \pm \sigma$ (8)	$\Delta F555W_{TO-HB} \pm \sigma$ (9)	$\Delta F555W_{TO-HB} \pm \sigma$ (10)	Age \pm error (11)	Age \pm error (12)	Age \pm error (13)	Age \pm error (14)
IC 4499	-1.50	-1.29	15.7	21.26	0.11	17.75	0.03	3.51	0.11	1.02	0.11	1.01	0.12
NGC 104	-0.71	-0.78	7.4	17.63	0.06	14.10	0.03	3.53	0.06	0.97	0.07	0.99	0.07
NGC 362	-1.33	-1.09	9.3	18.75	0.07	15.50	0.03	3.25	0.08	0.74	0.06	0.74	0.06
NGC 1261	-1.32	-1.08	18.2	20.11	0.05	16.85	0.03	3.26	0.06	0.75	0.05	0.75	0.05
NGC 1851	-1.23	-1.03	16.7	19.49	0.03	16.15	0.03	3.34	0.05	0.80	0.05	0.81	0.04
NGC 1904	-1.67	-1.37	18.8	19.61	0.08	16.25	0.03	3.36	0.09	0.90	0.08	0.87	0.08
NGC 2808	-1.36	-1.11	11.0	19.63	0.09	16.35	0.03	3.28	0.10	0.77	0.08	0.76	0.08
NGC 3201	-1.53	-1.24	9.0	18.08	0.04	14.85	0.03	3.23	0.05	0.77	0.04	0.73	0.04
NGC 4147	-1.77	-1.50	21.3	20.46	0.09	16.98	0.03	3.48	0.09	1.03	0.08	1.01	0.09
NGC 4372 *	-2.03	-1.88	7.1	18.94	0.05	15.58	0.03	3.36	0.06	0.98	0.05	0.98	0.05
NGC 4590	-2.11	-2.00	10.1	19.04	0.06	15.73	0.03	3.31	0.07	0.92	0.06	0.93	0.06
NGC 4833	-1.92	-1.71	6.9	19.14	0.05	15.70	0.03	3.44	0.06	1.01	0.05	1.00	0.06
NGC 5024	-2.04	-1.86	18.8	20.27	0.08	16.83	0.03	3.44	0.08	1.02	0.07	1.03	0.07
NGC 5694	-1.93	-1.74	29.1	22.01	0.08	18.53	0.03	3.48	0.08	1.05	0.07	1.05	0.07
NGC 5824	-1.85	-1.60	25.8	21.98	0.03	18.53	0.03	3.45	0.04	1.01	0.04	1.00	0.04
NGC 5904	-1.38	-1.12	6.2	18.49	0.07	15.15	0.03	3.34	0.08	0.83	0.07	0.81	0.07
NGC 5927 *	-0.32	-0.64	4.5	20.25	0.05	16.79	0.03	3.46	0.06	0.94	0.06	0.92	0.06
NGC 5946	-1.39	-1.22	7.4	21.01	0.15	17.60	0.03	3.41	0.15	0.90	0.14	0.89	0.15
NGC 5986	-1.65	-1.35	4.8	20.08	0.05	16.70	0.03	3.38	0.06	0.91	0.05	0.88	0.06
NGC 6171	-1.09	-0.95	3.3	19.23	0.07	15.70	0.03	3.53	0.07	0.98	0.07	0.99	0.08
NGC 6218	-1.40	-1.14	4.5	18.25	0.07	14.80	0.03	3.45	0.08	0.94	0.08	0.92	0.08
NGC 6235	-1.46	-1.18	2.9	20.41	0.14	17.00	0.03	3.41	0.15	0.91	0.14	0.89	0.15
NGC 6266	-1.23	-1.02	1.7	19.76	0.05	16.30	0.03	3.46	0.06	0.92	0.06	0.92	0.06
NGC 6273 *	-1.80	-1.53	1.6	19.95	0.04	16.55	0.03	3.40	0.05	0.96	0.03	0.93	0.04
NGC 6284	-1.24	-1.13	6.9	20.90	0.04	17.50	0.03	3.40	0.04	0.86	0.04	0.87	0.05
NGC 6287	-2.07	-1.91	1.7	20.59	0.11	17.13	0.03	3.46	0.12	1.05	0.11	1.06	0.11
NGC 6342	-0.66	-0.69	1.7	20.55	0.05	17.07	0.03	3.48	0.06	0.92	0.07	0.94	0.07
NGC 6362	-1.18	-0.99	5.3	18.88	0.03	15.42	0.03	3.46	0.04	0.91	0.04	0.92	0.04
NGC 6544 *	-1.48	-1.20	5.4	18.58	0.09	15.25	0.03	3.33	0.09	0.84	0.08	0.81	0.09
NGC 6584	-1.51	-1.30	7.0	19.94	0.10	16.60	0.03	3.34	0.10	0.85	0.09	0.83	0.09
NGC 6637	-0.72	-0.78	1.6	19.50	0.09	16.04	0.03	3.46	0.09	0.89	0.10	0.91	0.10
NGC 6652	-0.99	-0.97	2.4	19.52	0.06	16.06	0.03	3.46	0.07	0.89	0.07	0.92	0.07
NGC 6681	-1.64	-1.35	2.1	19.15	0.10	15.75	0.03	3.40	0.10	0.93	0.09	0.91	0.10
NGC 6717	-1.33	-1.09	2.3	19.24	0.07	15.80	0.03	3.44	0.08	0.92	0.08	0.91	0.08

Table 2—Continued

ID (1)	[Fe/H] _{ZW} (2)	[Fe/H] _{CG} (3)	r_{GC} (4)	$(F555W)_{TO} \pm \sigma$ (5)	$(F555W)_{HB} \pm \sigma$ (6)	$(F555W)_{HB} \pm \sigma$ (7)	$(F555W)_{HB} \pm \sigma$ (8)	$\Delta F555W_{TO-HB} \pm \sigma$ (9)	$\Delta F555W_{TO-HB} \pm \sigma$ (10)	Age \pm error (11)	Age \pm error (12)	Age \pm error (13)	Age \pm error (14)
NGC 6723	-1.12	-0.96	2.6	19.06	0.11	15.55	0.03	3.51	0.11	0.96	0.11	0.97	0.12
NGC 6838	-0.58	-0.73	6.7	18.01	0.05	14.54	0.03	3.47	0.06	0.91	0.06	0.92	0.06
NGC 6934	-1.54	-1.32	14.3	20.28	0.06	16.95	0.03	3.33	0.07	0.85	0.06	0.83	0.06
NGC 6981	-1.50	-1.21	12.9	20.22	0.08	16.90	0.03	3.32	0.08	0.83	0.07	0.80	0.08
NGC 7078	-2.13	-2.02	10.4	19.21	0.09	15.88	0.04	3.33	0.10	0.94	0.08	0.95	0.08
NGC 7089	-1.61	-1.31	10.4	19.44	0.10	16.03	0.03	3.41	0.11	0.94	0.10	0.91	0.11
NGC 7099	-2.05	-1.92	7.1	18.73	0.05	15.23	0.03	3.50	0.05	1.08	0.06	1.10	0.06

Table 3. Observational parameters and normalised ages for the groundbased data.

ID (1)	[Fe/H] _{ZW} (2)	[Fe/H] _{CG} (3)	r_{GC} (4)	$V_{TO} \pm \sigma$ (5) (6)	$V_{HB} \pm \sigma$ (7) (8)	$\Delta V_{TO-HB} \pm \sigma$ (9) (10)	Age \pm error (11) (12)	Age \pm error (13) (14)					
NGC 104	-0.71	-0.78	7.4	17.65	0.08	14.10	0.03	3.55	0.08	1.00	0.10	1.02	0.10
NGC 288	-1.40	-1.14	12.0	18.92	0.04	15.48	0.03	3.45	0.05	0.94	0.05	0.92	0.05
NGC 362	-1.33	-1.09	9.3	18.84	0.09	15.57	0.03	3.27	0.09	0.76	0.08	0.76	0.07
NGC 1261	-1.32	-1.08	18.2	19.98	0.06	16.74	0.03	3.24	0.07	0.74	0.05	0.74	0.05
NGC 1851	-1.23	-1.03	16.7	19.58	0.07	16.23	0.03	3.35	0.07	0.81	0.07	0.82	0.07
NGC 1904	-1.67	-1.37	18.8	19.62	0.09	16.25	0.03	3.37	0.10	0.91	0.09	0.88	0.09
NGC 2808	-1.36	-1.11	11.0	19.61	0.07	16.36	0.03	3.25	0.07	0.75	0.06	0.74	0.05
NGC 3201	-1.53	-1.24	9.0	18.11	0.05	14.83	0.03	3.28	0.06	0.80	0.05	0.77	0.05
NGC 4590	-2.11	-2.00	10.1	19.05	0.07	15.74	0.03	3.31	0.07	0.93	0.07	0.94	0.07
NGC 5053	-2.10	-1.98	16.8	20.00	0.06	16.64	0.03	3.37	0.07	0.99	0.05	1.01	0.05
NGC 5272	-1.66	-1.34	12.2	19.00	0.04	15.76	0.03	3.24	0.05	0.80	0.04	0.76	0.04
NGC 5466	-2.22	-2.20	16.2	19.89	0.07	16.50	0.03	3.39	0.07	1.01	0.06	1.03	0.06
NGC 5897	-1.93	-1.73	7.3	19.77	0.07	16.32	0.03	3.46	0.08	1.04	0.07	1.04	0.07
NGC 5904	-1.38	-1.12	6.2	18.47	0.03	15.12	0.03	3.34	0.04	0.83	0.04	0.81	0.04
NGC 6093	-1.75	-1.47	3.8	19.77	0.07	16.35	0.03	3.42	0.08	0.97	0.07	0.95	0.08
NGC 6121	-1.27	-1.05	5.9	16.87	0.03	13.43	0.03	3.44	0.04	0.91	0.04	0.91	0.04
NGC 6171	-1.09	-0.95	3.3	19.17	0.06	15.68	0.03	3.48	0.07	0.93	0.07	0.95	0.07
NGC 6205	-1.63	-1.33	8.7	18.53	0.06	15.01	0.03	3.52	0.07	1.05	0.07	1.02	0.07
NGC 6218	-1.40	-1.14	4.5	18.31	0.07	14.84	0.05	3.48	0.09	0.97	0.08	0.95	0.09
NGC 6254	-1.55	-1.25	4.6	18.48	0.05	15.11	0.05	3.37	0.07	0.89	0.06	0.86	0.07
NGC 6341	-2.24	-2.16	9.6	18.64	0.06	15.18	0.03	3.47	0.07	1.08	0.06	1.10	0.06
NGC 6362	-1.18	-0.99	5.3	18.86	0.08	15.43	0.03	3.43	0.08	0.88	0.09	0.89	0.09
NGC 6366	-0.58	-0.73	5.0	19.14	0.06	15.70	0.03	3.44	0.07	0.89	0.07	0.90	0.07
NGC 6397	-1.94	-1.76	6.0	16.44	0.04	13.03	0.03	3.41	0.05	1.00	0.03	0.99	0.05
NGC 6681	-1.64	-1.35	2.1	19.21	0.09	15.82	0.05	3.39	0.10	0.92	0.10	0.90	0.10
NGC 6723	-1.12	-0.96	2.6	19.07	0.09	15.53	0.03	3.54	0.09	0.99	0.10	1.01	0.10
NGC 6752	-1.54	-1.24	5.2	17.45	0.08	13.91	0.05	3.53	0.09	1.05	0.10	1.03	0.10
NGC 6809	-1.80	-1.54	3.9	17.93	0.12	14.44	0.03	3.49	0.12	1.05	0.12	1.04	0.13
NGC 6838	-0.58	-0.73	6.7	18.01	0.06	14.52	0.03	3.49	0.07	0.95	0.08	0.95	0.08
NGC 7078	-2.13	-2.02	10.4	19.24	0.06	15.89	0.03	3.35	0.07	0.97	0.06	0.98	0.06

